Neurobiology of Aging 73 (2019) 74–81

Contents lists available at ScienceDirect

Neurobiology of Aging

journal homepage: www.elsevier.com/locate/neuaging

Beta amyloid deposition maps onto hippocampal and subiculum atrophy in dementia with Lewy bodies

Elijah Mak [a], Paul C. Donaghy [b], Elizabeth McKiernan [a], Michael J. Firbank [b], Jim Lloyd [c], George S. Petrides [c], Alan J. Thomas [b], John T. O'Brien [a,*]

[a] Department of Psychiatry, University of Cambridge, Cambridge, UK
[b] Institute for Ageing and Institute of Neuroscience, Newcastle University, Newcastle upon Tyne, UK
[c] Nuclear Medicine Department, Newcastle Upon Tyne Hospitals, NHS Foundation Trust, Newcastle upon Tyne, UK

ARTICLE INFO

Article history:
Received 14 April 2018
Received in revised form 5 September 2018
Accepted 6 September 2018
Available online 12 September 2018

Keywords:
Dementia with Lewy bodies
Alzheimer's disease
Amyloid
PET
MRI

ABSTRACT

Although dementia with Lewy bodies (DLB) is a synucleinopathy, it is frequently accompanied by beta amyloid (Aβ) accumulation. Elucidating the relationships of Aβ with gray matter atrophy in DLB may yield insights regarding the contributions of comorbid Alzheimer's disease to its disease progression. Twenty healthy controls and 25 DLB subjects underwent clinical assessment, [^{18}F]-Florbetapir, and 3T magnetic resonance imaging. FreeSurfer was used to estimate cortical thickness and subcortical volumes, and PetSurfer was used to quantify [^{18}F]-Florbetapir standardized uptake value ratio. Principal component analysis was used to identify the dominant Aβ component for correlations with regional cortical thickness, hippocampal subfields, and subcortical structures. Relative to healthy controls, the DLB group demonstrated increased Aβ in widespread regions encompassing the frontal and temporoparietal cortices, whereas cortical thinning was restricted to the temporal lobe. Among DLB subjects, the Aβ component was significantly associated with more severe hippocampal and subiculum atrophy. These findings may reflect an early process of superimposed AD-like atrophy in DLB, thereby conferring support for the therapeutic potential of anti-Aβ interventions in people with DLB.

1. Introduction

Dementia with Lewy bodies (DLB) is the second most common degenerative form of dementia in elderly people after Alzheimer's disease (AD) (McKeith et al., 2017). Although alpha-synucleinopathy is recognized as the key neuropathological hallmark of DLB, up to 80% of people with DLB show varying degrees of AD pathologies—beta amyloid (Aβ) and neurofibrillary tau tangles (NFTs)—at autopsy (Colom-Cadena et al., 2013; McKeith et al., 2017, 2005). The advent of positron emission tomography (PET) amyloid ligands has offered unique opportunities for the antemortem quantification of Aβ burden and how it relates to clinical and neuroimaging abnormalities associated with preclinical and established AD (Chetelat et al., 2013; see Habib and Mak et al., 2017 for a systematic review). However, it remains unclear if and to what extent Aβ contributes to the disease progression and neurodegenerative changes in DLB (see Donaghy et al., 2015 for a systematic review). This knowledge gap is unfortunate because new insights concerning the impact of Aβ in DLB could have long-term ramifications on treatment strategies and monitoring outcomes in emerging trials that specifically target the aggregation of Aβ (Sperling et al., 2014).

The "Aβ cascade hypothesis" in AD posits an initiating event of amyloidosis, with subsequent tau accumulation preceding downstream brain atrophy and cognitive decline (Hardy, 2002). This AD spatiotemporal model of disease progression has been central to the recent shift toward disease-modification strategies (Sperling et al., 2014), although its relevance to DLB is still controversial (Donaghy et al., 2015). For instance, limited evidence suggests a modest association of Aβ with cognitive decline and increased mortality risks (Gomperts, 2014), although others have reported no association with dementia severity in DLB (Shimada et al., 2013). The discordant findings may, in part, stem from the inherent challenges of psychometric assessments such as mood changes, fatigue, and attentional impairments, all of which could be exacerbated by cognitive fluctuations in DLB patients. In contrast, particularly in the context of AD, brain atrophy is increasingly proposed as a reliable biomarker of disease progression (Sluimer et al., 2008) and a secondary outcome measure in clinical trials (Cash et al., 2015; Schott et al., 2010; Slattery et al., 2015). Widely understood to be one of the endpoints in the neurodegenerative cascade (Jack et al., 2013), brain atrophy has been extensively studied in relation to upstream Aβ across the spectrum of normal

* Corresponding author at: Foundation Professor of Old Age Psychiatry, Department of Psychiatry, University of Cambridge School of Clinical Medicine, Box 189, Level E4 Cambridge Biomedical Campus, Cambridge, CB2 0SP, UK. Tel.: +44 (0) 1223 336968; fax: +44 (0) 1223 336581.
E-mail address: john.obrien@medschl.cam.ac.uk (J.T. O'Brien).

0197-4580/$ – see front matter © 2018 Elsevier Inc. All rights reserved.
https://doi.org/10.1016/j.neurobiolaging.2018.09.004

aging, mild cognitive impairment, and AD (Chetelat et al., 2010; Josephs et al., 2008). Surprisingly, this question has been scarcely addressed in DLB (Sarro et al., 2016; Shimada et al., 2013; see Table 1 for main findings).

A voxel-based morphometry analysis reported a stereotypical AD pattern of parahippocampal atrophy in a small sample of antecedent Aβ-positive patients with DLB (Shimada et al., 2013). This observation is broadly consistent with another longitudinal study, where higher baseline levels of global [^{11}C]-Pittsburgh Compound B binding were associated with higher rates of atrophy in the medial temporal lobe and other cortical regions in DLB over 2 years (Sarro et al., 2016). In both studies, the authors interpreted their findings to suggest that people with DLB may stand to benefit from antiamyloid therapies should such treatments be available and safe. However, the sample size was rather small in both studies, and no controls were recruited (Sarro et al., 2016) Finally, no study has evaluated the relationships of Aβ burden with hippocampal subfields. Postmortem investigations have demonstrated that hippocampal atrophy in AD is nonuniform, with preferential vulnerability of the cornu ammonis 1 (CA1) and subiculum atrophy in early AD (Braak and Braak, 1991; West et al., 1994). Therefore, understanding how Aβ relates to hippocampal subfields may provide novel insights about the pathological underpinnings of early AD-type atrophy in people with DLB. To these ends, automated techniques have been validated to perform segmentation of hippocampal subfields from structural magnetic resonance imaging (MRI) data (Iglesias et al., 2015; Wisse et al., 2014; Yushkevich et al., 2015). We and others have previously applied the FreeSurfer technique to demonstrate differential hippocampal subfield atrophy in DLB and AD (Chow et al., 2012; Mak et al., 2016), achieving very similar findings compared to our manual tracing work (Firbank et al., 2010).

To extend these promising investigations and clarify the topography of Aβ-associated atrophy patterns in DLB, we performed a PET-computed tomography (PET-CT) and structural MRI study with the following key aims: (1) To compare and contrast the spatial profiles of abnormal Aβ accumulation and cortical thinning in DLB relative to healthy controls; (2) to determine the global overlap between Aβ binding and cortical thinning, and (3) to delineate the associations of a data-driven composite measure of Aβ burden with regional cortical thickness, hippocampal subfield, and other subcortical structures.

2. Methods

2.1. Participants

Participants were recruited prospectively between June 2013 and February 2016 from secondary care services in the North of England. Control subjects were recruited through a research case register or were partners of participants. All subjects were ≥60 years old. Dementia subjects had a diagnosis of probable DLB confirmed by 2 clinicians based on current diagnostic criteria with a mini-mental state examination (MMSE) score ≥12. Results of amyloid imaging were not known to the clinicians when making the diagnosis. Control subjects had an MMSE score ≥26 and no signs of dementia. DLB subjects were recruited before the publication of the 2017 diagnostic criteria for DLB; however, they also satisfied the updated criteria for probable DLB (McKeith et al., 2017). Subjects were excluded if they had a major concurrent psychiatric illness, severe physical illness, contraindications to PET-CT imaging, a history of other significant neurological illness including stroke, previous experimental treatment with an amyloid-targeting agent, or current treatment with any other investigational agent. Subjects with capacity gave their written informed consent to take part in the study. For those with dementia who lacked capacity, their participation in the study was discussed with a consultee in accordance with the Mental Capacity Act. The study received ethical approval from the National Research Ethics Service Committee North East—Newcastle and North Tyneside 2 (Research Ethics Committee Identification Number 13/NE/0064).

2.2. Baseline cognitive and clinical assessment

The DLB sample underwent clinical and cognitive assessments, including the Addenbrooke's Cognitive Examination-Revised and the Revised Unified Parkinson's disease Rating Scale Motor Subscale (UPDRS).

2.3. Structural MRI

Scans were acquired on a 3T whole body MR scanner (Achieva scanner; Philips Medical Systems), with body coil transmission and 8 channel head coil receiver. Images acquired included a 3D sagittal magnetization-prepared rapid gradient echo (MPRAGE) sequence (repetition time 8.3 ms, echo time 4.6 ms, flip angle 8^{o}, inversion delay 1250 ms, imaging time 4.5 mins). The sagittal acquisition matrix was 216 × 240, giving a voxel size of 1 × 1 × 1 mm. The T1-MPRAGE data were processed using FreeSurfer version 6 to obtain cortical thickness measurements in 34 regions of interest (ROIs) per hemisphere, based on the Desikan-Killiany parcellation scheme (Desikan et al., 2006). The technical details for the quantification of cortical thickness have been extensively described (Fischl and Dale, 2000). Briefly, for each T1-MPRAGE data, the pial and white matter surfaces were generated, and the cortical thickness was measured as the distance between the boundaries of pial and white matter surfaces. Visual inspection was carried by 2 operators (EM and EMc) while blinded to group diagnostic information, and corrections were performed to ensure accurate skull-stripping, placement of control

Table 1
Summary of main findings from previous studies investigating the association of [^{11}C]-PiB binding to gray matter atrophy in DLB

Authors	Sample characteristics	Study design and imaging analyses	Summary of main findings
Shimada et al., 2013	17 HC age: 68 y, MMSE score: 28	Cross-sectional analysis	Aβ+ DLB/PDD subjects showed parahippocampal, lateral temporal, and parietal atrophy.
	8 DLB, 7 PDD age: 73 y, MMSE score: 22	Voxel-based morphometry	Aβ- DLB/PDD did not exhibit significant atrophy.
	13 AD age: 76 y, MMSE: 20 score	Partial volume was not performed on [^{11}C]-PiB data	Mean [^{11}C]-PiB SUVR did not correlate with voxelwise gray matter maps.
Sarro et al., 2016	20 DLB age: 70 y, MMSE score: 22	Longitudinal within-group design Time between MRI scans: 2.5 y ROI analysis between global [^{11}C]-PiB uptake and rate of atrophy in gray matter ROIs, controlled for age	Higher baseline [^{11}C]-PiB SUVR was associated with accelerated GM atrophy over time in multiple regions, such as the posterior cingulate cortex, medial temporal lobe, occipital lobe, caudate and putamen, and ventricular enlargement

Key: Aβ, beta amyloid; DLB, dementia with Lewy bodies; GM, gray matter; HC, healthy controls; MMSE, mini-mental state examination; MRI, magnetic resonance imaging; PDD, Parkinson's disease with dementia; PiB, Pittsburgh Compound B; ROI, region of interest; SUVR, standardized uptake ratios; VBM, voxel-based morphometry.

points, and reconstruction of white matter and pial surfaces. Five DLB subjects were excluded in the process. The cortical thickness maps were smoothed using a Gaussian kernel across the surface with a full width at half maximum of 15 mm. In addition, the volumetric pipeline of FreeSurfer was used to estimate the total intracranial volumes (ICVs), as well as the subcortical deep gray matter regions: thalamus, nucleus accumbens, amygdala, pallidum, putamen, caudate, and the hippocampus. Hippocampal subfield volumes were estimated using FreeSurfer. Briefly, this automated technique uses a probabilistic atlas built upon ultrahigh-resolution *ex vivo* MRI data (Iglesias et al., 2015). Compared to its previous version (Van Leemput et al., 2009), the ultrahigh resolution of the *ex vivo* MRI training data provided a better contrast between the subfield boundaries, thus improving the reliability of the subfield annotations. As a result, the subfield volumes estimated from this technique yielded better agreement with those from histological studies (Iglesias et al., 2015). To facilitate the integration of PET and MRI data, we used the PetSurfer tool to segment additional regions from the T1 MRI data, such as the cerebrospinal fluid (CSF), pons, skull, and air cavities. These additional segmentations were merged with the default FreeSurfer segmentations to provide anatomical information for partial-volume correction (PVC) described below (Greve et al., 2014).

2.4. PET imaging

PET-CT imaging was performed using a Siemens Biograph-40 PET-CT scanner. Subjects had a 15-minute scan 30–50 minutes after a 370 MBq intravenous injection of [^{18}F]-Florbetapir (Amyvid). PET images were reconstructed using iterative reconstruction (4 iterations, 16 subsets), with a 168 × 168 matrix size, 2.04 × 2.04 mm pixel size, 3 mm slice thickness, and a 3 mm postreconstruction Gaussian filter. Attenuation correction was performed using CT scan data obtained immediately before the PET images and reconstructed with 3-mm slice thickness to match the PET images. To perform PVC, each frame of the [^{18}F]-Florbetapir data was realigned with statistical parametric mapping and averaged. The resultant mean images were coregistered to their native T1 MRI data and the accuracy of the PET-MRI registration was inspected for each subject. Consistent with previous studies (Greve et al., 2016; LaPoint et al., 2017), the Symmetric Geometric Transfer Matrix technique was implemented to derive PVC-ROIs after the FreeSurfer segmentations were transformed back into the PET native space. Subsequently, the standardized uptake ratios (SUVRs) were obtained for each region by normalization against the cerebellar cortex. Notably, this approach in FreeSurfer has been demonstrated to show an excellent agreement of PET regional quantification with manually defined regions (Su et al., 2013). As the Symmetric Geometric Transfer Matrix technique is strictly designed for PVC of ROI data, we used the Muller-Gartner technique to perform PVC on vertexwise [^{18}F]-Florbetapir data (Greve et al., 2014). The corrected vertexwise PET data were then sampled onto the cortical surface and smoothed using a full width at half maximum of 4 mm. By restricting the smoothing along the cortical ribbon, we further account for the contamination of [^{18}F]-Florbetapir signal due to contributions from the white matter, CSF, or adjacent gray matter regions that are highly proximal in Euclidean space. Compared to volumetric methods, the surface-based PET framework is increasingly advocated for parametric comparisons as it has been associated with reductions of intersubject variance and higher reliability across different tracers and PET systems (Greve et al., 2014; Matheson et al., 2017).

2.5. Statistical analyses

Statistical analyses were performed in MATLAB 2017A and the R statistical package. The specific analyses catering to each of our primary objectives are detailed as follows: To characterize the spatial distribution of increased Aβ and cortical thinning in DLB, both vertexwise [^{18}F]-Florbetapir PET and cortical thickness data were compared between the DLB and healthy controls using the general linear model in FreeSurfer and were adjusted for age and corrected for multiple comparisons using the clusterwise method. The vertexwise threshold, otherwise referred to as the cluster-forming threshold, was set at 0.001, whereas significance for clusters was set at $p < 0.05$. Next, using an ROI-based approach, we explored the inter-regional correlation between [^{18}F]-Florbetapir SUVR and cortical thickness (i.e., 68 ROIs per modality) with linear mixed effect models using the lme4 package in R (Bates et al., 2015). Specifically, cortical thickness was assigned as the dependent variable, with [^{18}F]-Florbetapir SUVR ROIs as fixed factors, allowing for random intercepts across subjects and cortical lobes (i.e., frontal, occipital, parietal, and temporal lobes) so as to account for the interdependency resulting from repeated measurements per subject (i.e., 68 ROIs per subject). The statistical significance of the relationships was assessed using the likelihood ratio test by comparing the fit between the full linear mixed effect model and a reduced model (i.e., without the fixed effect of [^{18}F]-Florbetapir SUVR ROIs (Bates et al., 2015)). The [^{18}F]-Florbetapir SUVR data set across the DLB subjects was first subjected to a principal component analyses (PCAs) to identify the composite factors that represent the dominant topography of [^{18}F]-Florbetapir SUVR in the DLB sample (i.e., the weighted combination of Aβ binding in brain regions that account for the most variance across the DLB subjects). The resulting score for each DLB subject could be interpreted as a data-driven composite measure of [^{18}F]-Florbetapir SUVR (Supplementary Fig. 1). Subsequently, the amyloid PCA was correlated with regional cortical thickness (68 ROIs), total hippocampus, CA1, and subiculum while adjusting for age and total ICVs for subcortical volumes. The a priori selected hippocampal ROIs were the total hippocampus, CA1, and the total subiculum. To account for multiple correlations, the statistical threshold for significance was set at the Benjamini-Hochberg false discovery rate (FDR)-adjusted level of $p < 0.05$ (i.e., across 68 ROIs for cortical thickness). The statistical significance threshold was set to $p < 0.05$ for all other tests.

3. Results

3.1. Clinical and demographic information

The brief clinical and cognitive characteristics of the included sample are shown in Table 2. Both the DLB and healthy controls were well matched in terms of age and gender. As expected, the DLB group scored significantly poorer on the Addenbrooke's Cognitive Examination-Revised and worse on the UPDRS ($p < 0.001$). To determine whether the exclusion of 5 DLB subjects had a significant impact on the demographics and cognitive characteristics in the study sample, we also compared these variables in the full data set and found similar results: Both the DLB and healthy control groups

Table 2
Brief demographics and cognitive characteristic of the study sample

Variables	Healthy controls (n = 20)	DLB (n = 25)	*p* value
Age	75.9 ± 7.3	75.4 ± 6.8	0.8[a]
Gender (male:female)	16:4	21:4	0.7[b]
ACER	94.8 ± 3.02	65 ± 15.2	<0.001[c]
UPDRS	5.6 ± 3.5	42.9 ± 18.4	<0.001[c]

Key: ACER, Addenbrooke's Cognitive Examination-Revised; DLB, dementia with Lewy bodies; UPDRS, Revised Unified Parkinson's disease Rating Scale Motor Subscale.
[a] Student's *t*-test.
[b] χ^2 test.
[c] Rank sum test.

were still comparable in terms of age and gender, although MMSE and UPDRS remained significantly poorer in the DLB group ($p < 0.001$) (Supplementary Table 1).

3.2. Vertexwise comparisons

Compared to the total sample of healthy controls (n = 20), the DLB group demonstrated significantly increased Aβ in widespread regions encompassing the frontal and temporoparietal cortices (adjusted for age and Monte Carlo clusterwise correction: $p_{\text{vertex-wise}} < 0.001$, $p_{\text{cluster-wise}} < 0.05$). Next, we compared cortical thickness in DLB relative to amyloid-negative healthy controls (n = 16). The DLB group showed significant cortical thinning predominantly in the temporal cortex (adjusted for age and Monte Carlo clusterwise correction: $p_{\text{vertex-wise}} < 0.001$, $p_{\text{cluster-wise}} < 0.05$). Both the uncorrected and corrected vertexwise contrast maps are shown in Fig. 1.

3.3. Comparison of total hippocampus and hippocampal subregions

After accounting for age and ICVs, the DLB group showed significantly smaller volumes relative to the amyloid-negative healthy controls in the hippocampus ($p < 0.01$) and CA1 ($p = 0.02$) and while subiculum differences approached trend ($p = 0.06$) (Fig. 2).

3.4. Global relationship between Aβ and cortical thinning

Mixed effect models showed a weak but significant relationship between [^{18}F]-Florbetapir SUVR and cortical thinning across the cortex in the DLB sample [$\beta = -0.1$, SE = 0.02, T = −5.3] (Fig. 3). The statistical significance of this global relationship was inferred from a χ^2 comparison of the log-likelihood values against the reduced null model ($p < 0.001$).

3.5. Principal component analysis of [^{18}F]-Florbetapir in DLB and its association with gray matter atrophy

Across the [^{18}F]-Florbetapir SUVRs in the brain regions, PCA was first applied to reduce the dimensionalities of the [^{18}F]-Florbetapir data into component topographies, effectively accounting for the high collinearity of the [^{18}F]-Florbetapir data across ROIs. The PCA revealed a principal Aβ component that was characterized by positive regional loadings in the bilateral precuneus and frontal cortices (79% explained variance) (Fig. 4). We did not find any association of the Aβ principal component with regional cortical thickness after FDR correction. The PCA was significantly associated with more severe hippocampal ($r = -0.5$, $p^{FDR} = 0.03$) and subiculum atrophy ($r = -0.6$, $p^{FDR} = 0.01$) after controlling for ICV and age (Fig. 5). To ensure that findings were robust across different techniques, we repeated the analyses using the MGX technique for PVC and obtained consistent results (Supplementary Fig. 3).

4. Discussion

Clarifying the in vivo relationships between Aβ and brain atrophy in DLB will help stratify at-risk persons and identify vulnerable patients who would stand to benefit from future antiamyloid therapies should they prove to be effective. To this end, we performed a thorough mapping of Aβ on gray matter atrophy in the largest sample of DLB patients to undergo amyloid PET imaging and structural MRI to date. Overall, our main findings demonstrated that (1) the spatial extent of abnormal Aβ accumulation is much wider than the spatial extent of cortical thinning, congruent with conceptual biomarker models that confer primacy of Aβ deposition with respect to brain atrophy, (2) the global topography of Aβ showed a modest overlap with cortical thinning across the brain, (3) at the regional level, however, Aβ is preferentially associated with hippocampal and subiculum atrophy—both of which are markers of early vulnerability in AD. These findings, along with others (Sarro et al., 2016), appear to support the therapeutic potential of emerging anti-Aβ treatments in DLB.

In our study, the integration of PET and structural MRI data afforded the opportunity to jointly compare the intensity and spatial profiles of abnormal Aβ and cortical thinning within the same DLB subjects against a group of healthy controls who were comparable in terms of age and gender. Our observations of increased Aβ aggregation spanning the inferior temporal and posterior parietal cortices and the medial frontal regions are in accordance with previous studies using the [^{11}C]-Pittsburgh Compound B

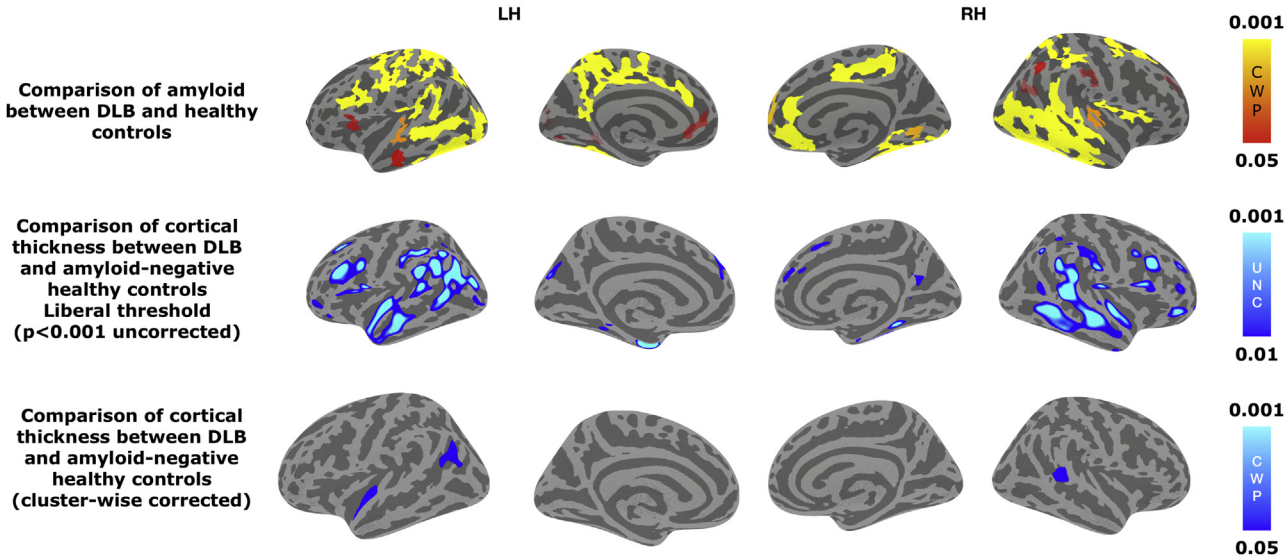

Fig. 1. Vertexwise comparison of [^{18}F]-Florbetapir SUVR and cortical thickness in DLB against amyloid-negative healthy controls. Compared to healthy controls, DLB showed significantly increased accumulation of Aβ in multiple cortices spanning the frontal and temporoparietal regions. Compared to amyloid-negative healthy controls, cortical thinning in DLB was restricted to the temporal cortices. Abbreviations: Aβ, beta amyloid; DLB, dementia with Lewy bodies; SUVR, standardized uptake ratio.

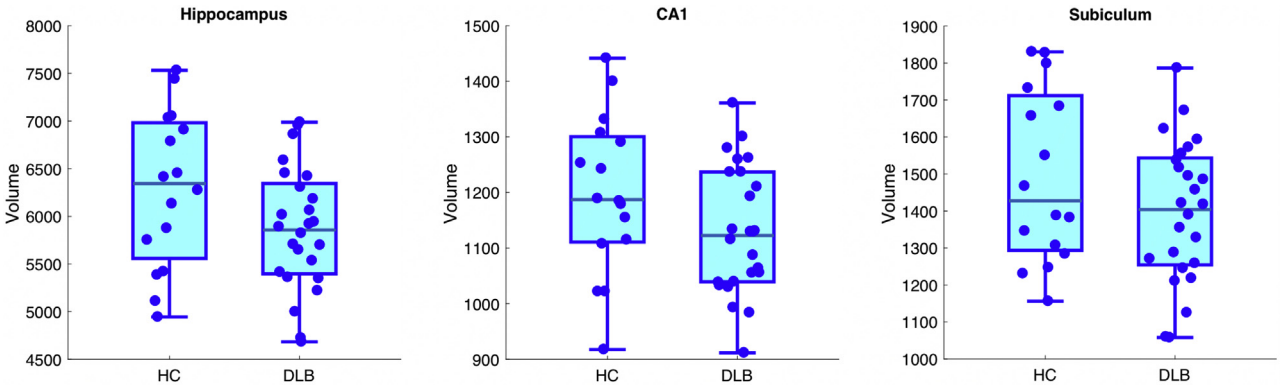

Fig. 2. Box plot of total volumes in the hippocampus, CA1, and subiculum in DLB and amyloid-negative healthy controls. Abbreviations: CA1, cornu ammonis 1; DLB, dementia with Lewy bodies; HC, healthy controls.

tracer (Gomperts et al., 2012, 2008), and together confirm that cortical Aβ is a common feature of DLB that can be detected in vivo. In contrast, the pattern of cortical thinning was constrained to the temporal cortex in our sample of DLB. Indeed, the stark disparity between the spatial extent of Aβ accumulation and cortical thinning is in keeping with the biomarker model in AD (Jack et al., 2013).

Set against the putative model of disease progression in AD, we aimed to determine the global overlap between Aβ burden and cortical thinning by using mixed effect models. Interestingly, our whole-brain, inter-regional analyses showed that elevated Aβ binding was associated with cortical thinning particularly in the temporal lobe (Fig. 3), where a focal cluster of significant atrophy was found in DLB compared to healthy controls (Fig. 1). Bearing in mind the absence of a longitudinal design in the present study, it is conceivable that the cortical distribution of antecedent Aβ may shape downstream patterns of cortical thinning in DLB, with the temporal lobe being the most susceptible to the neurotoxicity induced by early Aβ. Nevertheless, the weak effect size of the mixed effect model hints that other pathological factors—such as tau and

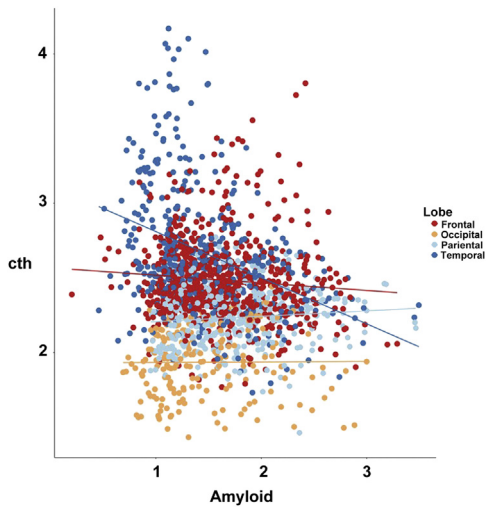

Fig. 3. Global relationship between amyloid and cortical thinning across the cortex. Each data point represents a subject-specific region of interest (ROI) from the Desikan-Killiany template (25 DLB subjects * 68 ROIs for amyloid and cortical thickness across the whole brain) and colored according to the cortical lobes. Mixed effect models revealed a modest but significant relationship between increased [^{18}F]-Florbetapir SUVR and cortical thinning. Abbreviations: DLB, dementia with Lewy bodies; SUVR, standardized uptake ratio.

Lewy bodies—may still influence atrophy to a larger degree than Aβ deposits.

After establishing the topological overlap between increased Aβ binding and cortical thinning, we aimed to determine the extent to which the overall intensity of Aβ is correlated with regional cortical thickness in DLB. Multivariate PCA was first used to identify the most dominant pattern of Aβ in our DLB sample. Unbiased against anatomical definitions, multivariate techniques such as PCA evaluate the covariance structure of the PET data across brain regions rather than proceeding on a region-by-region basis (i.e., conventional univariate analyses). The principal Aβ component was characterized by higher loadings within the bilateral precuneus and frontal cortices, remarkably mirroring the stereotypical distribution of Aβ in sporadic AD (Brier et al., 2016). This suggests a similar cortical pattern of Aβ binding in DLB and AD, although absolute levels of Aβ are typically less severe in DLB relative to AD (Donaghy et al., 2015). Consistent with a previous study (Shimada et al., 2016), we did not observe any robust correlations between Aβ and regional cortical thinning. However, the Aβ component was inversely associated with hippocampal and subiculum atrophy—both of which are widely recognized as early structural biomarkers of AD (de Flores et al., 2015; Mak et al., 2017a). This subiculum finding is especially noteworthy considering the growing research interest in hippocampal subfields, which may provide unique disease-related insights beyond the total hippocampus (de Flores et al., 2015; Firbank et al., 2010; Mak et al., 2017b). Indeed, the subicular complex was previously reported as the earliest marker of AD (Carlesimo et al., 2015). Taken together with our findings, DLB patients with greater manifestation of the principal Aβ component are more likely to exhibit atrophy patterns associated with early AD. These findings also confirmed previous reports where higher cortical Aβ was associated with greater temporal lobe atrophy (Sarro et al., 2016; Shimada et al., 2016). Furthermore, the absence of correlations between the Aβ component and other subcortical structures guards against the possibility that our correlational findings are merely reflecting a generalized pattern of Aβ-associated atrophy.

Nevertheless, these cross-sectional correlations should not be taken as evidence for a sole contribution of Aβ to drive atrophy in DLB. Indeed, several lines of research indicate that such conclusions may be oversimplified: (1) previous autoradiographic analysis in AD has reported intense tau inclusions ([^{11}C]-PBB3 ligand) in the subiculum without noticeable binding of [^{11}C]-Pittsburgh Compound B (Maruyama et al., 2013); (2) we have previously reported that NFTs predicted medial temporal lobe atrophy independent of Aβ plaques in DLB cases (Burton et al., 2009); (3) in vivo studies in

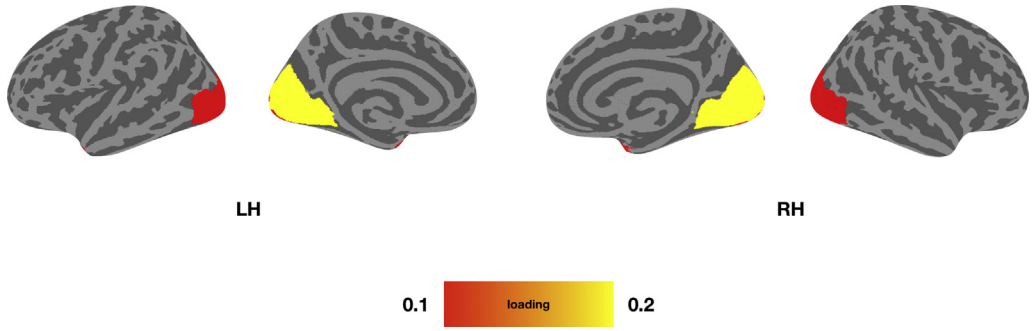

Fig. 4. Multivariate principal component analysis of [^{18}F]-Florbetapir SUVR in DLB. The first identified component of Aβ in DLB explained 79% of the variance. It is characterized by prominent loadings within the bilateral precuneus and frontal cortices, mirroring the characteristic topography of Aβ observed in sporadic AD. Abbreviations: Aβ, beta amyloid; AD, Alzheimer's disease; DLB, dementia with Lewy bodies; SUVR, standardized uptake ratio.

preclinical AD have reported that CSF tau modulates the relationship between Aβ and brain atrophy (Fortea et al., 2014). Furthermore, given the limited spatial resolution of PET, we could not determine whether hippocampal and subiculum atrophy are associated with focal [^{18}F]-Florbetapir binding within the same regions. Therefore, considering the growing body of evidence implicating early hippocampal and subiculum atrophy in AD (see de Flores et al., 2015 for a systematic review), the present findings may reflect an early process of AD-like atrophy emerging from the synergistic interactions of Aβ and NFTs. Ultimately, longitudinal designs with serial PET imaging of Aβ and NFTs will be necessary to validate this hypothesis.

5. Conclusion

Understanding the role of Aβ in people with DLB during life has implications for patient stratification and the optimal design of clinical trials assessing antiamyloid therapies. In the first report of its kind in DLB, our study demonstrated an association of the principle component of Aβ deposition with hippocampal and subiculum atrophy in DLB. We propose that Aβ maps onto atrophy in susceptible regions that are among the first to undergo neurodegeneration in AD and concur with previous recommendations for investigating the efficacy of anti-Aβ therapeutics in people with DLB (Gomperts, 2014; Sarro et al., 2016; Shimada et al., 2013). Despite the high-profile failures of anti-Aβ treatments in people with AD, there are several reasons as to why DLB patients may stand to benefit from such treatments. First, it is well established that macroscopic neurodegeneration is relatively milder in DLB compared to AD (Mak et al., 2015a; Nedelska et al., 2015). To the extent that the effectiveness of disease modification depends on the preservation of brain structure, it is conceivable that treatments may work better in DLB than in AD, where irreversible and extensive brain atrophy may pose insurmountable challenges for any drug to induce meaningful cognitive benefits. Taking a long-term perspective, future progress in disease-modification trials for AD may also be generalizable for people with DLB because there is emerging evidence—such as provided in this study and others—arguing that coexistent Aβ is not a benign process in DLB but one that may be associated with an AD type of brain atrophy.

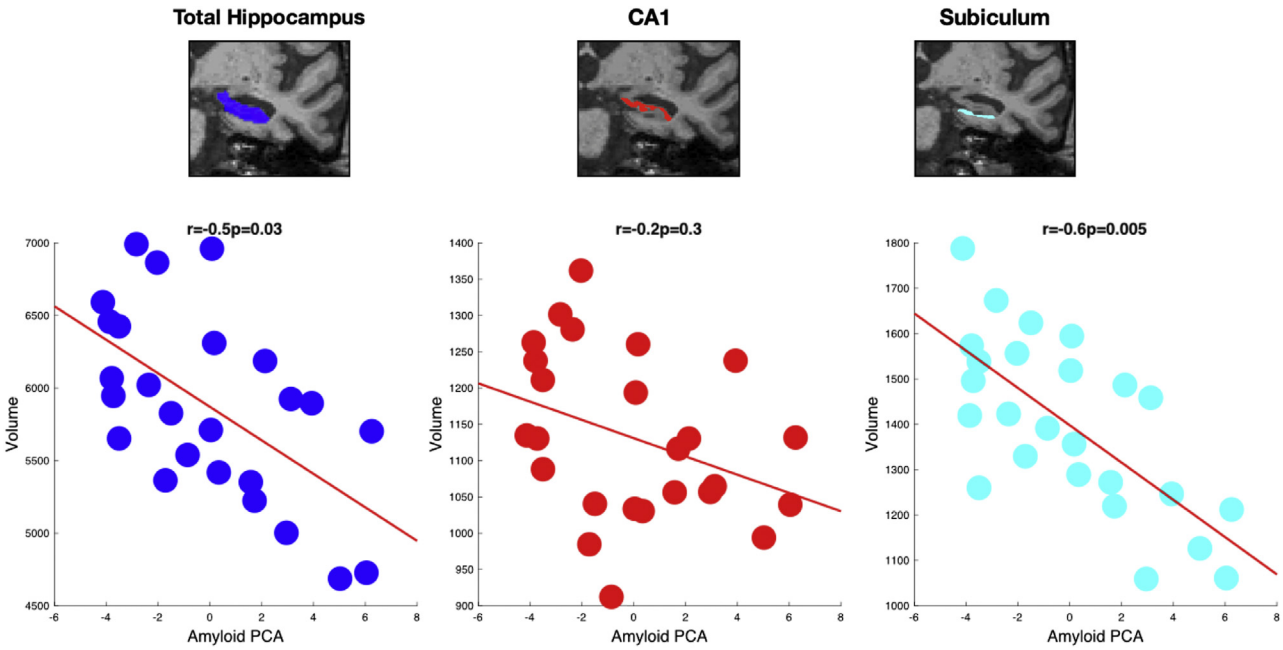

Fig. 5. Correlation between Aβ principal component and volume of hippocampal subfields. Across the DLB subjects, greater representation of the Aβ principal component was significantly correlated with the smaller hippocampus and subiculum. No signification correlations were found with other subcortical structures. Abbreviations: Aβ, beta amyloid; DLB, dementia with Lewy bodies; PCA, principal component analysis.

Clinical trials are warranted to establish whether anti-Aβ treatments could be recommended as an additional intervention as a part of a multicombinatorial treatment strategy targeting various aspects of DLB. Moving forward, future studies incorporating multi-PET imaging for tau and alpha-synuclein would be critical to disentangle the respective contributions of different pathologies to the multifaceted clinical picture of DLB.

Disclosure statement

The authors confirm they do not have any financial or personal conflict of interests.

Acknowledgements

The authors would like to thank the staff of the NIHR Clinical Research Network North East and Cumbria for their invaluable support with participant recruitment for this study.

The authors thank Avid, a wholly owned subsidiary of Eli Lilly and Company, for supply of Florbetapir and for financial support for the study. This research study was supported by the NIHR Newcastle Biomedical Research Center.

Appendix A. Supplementary data

Supplementary data to this article can be found online at https://doi.org/10.1016/j.neurobiolaging.2018.09.004.

References

Bates, D., Mächler, M., Bolker, B., Walker, S., 2015. Fitting linear mixed-effects models using lme4. J. Stat. Softw. 67, 1–48.

Braak, H., Braak, E., 1991. Neuropathological stageing of Alzheimer-related changes. Acta Neuropathol. 82, 239–259.

Brier, M.R., Gordon, B., Friedrichsen, K., McCarthy, J., Stern, A., Christensen, J., Owen, C., Aldea, P., Su, Y., Hassenstab, J., Cairns, N.J., Holtzman, D.M., Fagan, A.M., Morris, J.C., Benzinger, T.L., Ances, B.M., 2016. Tau and A-beta imaging, CSF measures, and cognition in Alzheimer's disease. Sci. Transl. Med. 8, 1–10.

Burton, E.J., Barber, R., Mukaetova-Ladinska, E.B., Robson, J., Perry, R.H., Jaros, E., Kalaria, R.N., O'Brien, J.T., 2009. Medial temporal lobe atrophy on MRI differentiates Alzheimer's disease from dementia with Lewy bodies and vascular cognitive impairment: a prospective study with pathological verification of diagnosis. Brain 132, 195–203.

Carlesimo, G.A., Piras, F., Orfei, M.D., Iorio, M., Caltagirone, C., Spalletta, G., 2015. Atrophy of presubiculum and subiculum is the earliest hippocampal anatomical marker of Alzheimer's disease. Alzheimers Dement. (Amst.) 1, 24–32.

Cash, D.M., Frost, C., Iheme, L.O., Ünay, D., Kandemir, M., Fripp, J., Salvado, O., Bourgeat, P., Reuter, M., Fischl, B., Lorenzi, M., Frisoni, G.B., Pennec, X., Pierson, R.K., Gunter, J.L., Senjem, M.L., Jack, C.R., Guizard, N., Fonov, V.S., Collins, D.L., Modat, M., Cardoso, M.J., Leung, K.K., Wang, H., Das, S.R., Yushkevich, P.A., Malone, I.B., Fox, N.C., Schott, J.M., Ourselin, S., 2015. Assessing atrophy measurement techniques in dementia: results from the MIRIAD atrophy challenge. Neuroimage 123, 149–164.

Chetelat, G., La Joie, R., Villain, N., Perrotin, A., De La Sayette, V., Eustache, F., Vandenberghe, R., 2013. Amyloid imaging in cognitively normal individuals, at-risk populations and preclinical Alzheimer's disease. Neuroimage Clin. 2, 356–365.

Chetelat, G., Villemagne, V.L., Bourgeat, P., Pike, K.E., Jones, G., Ames, D., Ellis, K.A., Szoeke, C., Martins, R.N., O'Keefe, G.J., Salvado, O., Masters, C.L., Rowe, C.C., 2010. Relationship between atrophy and beta-amyloid deposition in Alzheimer disease. Ann. Neurol. 67, 317–324.

Chow, N., Aarsland, D., Honarpisheh, H., Beyer, M.K., Somme, J.H., Elashoff, D., Rongve, A., Tysnes, O.B., Thompson, P.M., Apostolova, L.G., 2012. Comparing hippocampal atrophy in Alzheimer's dementia and dementia with lewy bodies. Dement. Geriatr. Cogn. Disord. 34, 44–50.

Colom-Cadena, M., Gelpi, E., Charif, S., Belbin, O., Blesa, R., Marti, M.J., Clarimon, J., Lleo, A., 2013. Confluence of alpha-synuclein, tau, and beta-amyloid pathologies in dementia with Lewy bodies. J. Neuropathol. Exp. Neurol. 72, 1203–1212.

de Flores, R., La Joie, R., Landeau, B., Perrotin, A., Mézenge, F., de La Sayette, V., Eustache, F., Desgranges, B., Chételat, G., 2015. Effects of age and Alzheimer's disease on hippocampal subfields. Hum. Brain Mapp. 36, 463–474.

Desikan, R.S., Ségonne, F., Fischl, B., Quinn, B.T., Dickerson, B.C., Blacker, D., Buckner, R.L., Dale, A.M., Maguire, R.P., Hyman, B.T., Albert, M.S., Killiany, R.J., 2006. An automated labeling system for subdividing the human cerebral cortex on MRI scans into gyral based regions of interest. Neuroimage 31, 968–980.

Donaghy, P., Thomas, A.J., O'Brien, J.T., 2015. Amyloid PET imaging in Lewy body disorders. Am. J. Geriatr. Psychiatry 23, 23–37.

Firbank, M.J., Blamire, A.M., Teodorczuk, A., Teper, E., Burton, E.J., Mitra, D., O'Brien, J.T., 2010. High resolution imaging of the medial temporal lobe in Alzheimer's disease and dementia with Lewy bodies. J. Alzheimers. Dis. 21, 1129–1140.

Fischl, B., Dale, A.M., 2000. Measuring the thickness of the human cerebral cortex from magnetic resonance images. Proc. Natl. Acad. Sci. U. S. A. 97, 11050–11055.

Fortea, J., Vilaplana, E., Alcolea, D., Carmona-Iragui, M., Sánchez-Saudinos, M.B., Sala, I., Antón-Aguirre, S., González, S., Medrano, S., Pegueroles, J., Morenas, E., Clarimón, J., Blesa, R., Lleó, A., 2014. Cerebrospinal fluid β-amyloid and phospho-tau biomarker interactions affecting brain structure in preclinical Alzheimer disease. Ann. Neurol. 76, 223–230.

Gomperts, S.N., 2014. Imaging the role of amyloid in PD dementia and dementia with Lewy bodies. Curr. Neurol. Neurosci. Rep. 14, 472.

Gomperts, S.N., Locascio, J.J., Marquie, M., Santarlasci, A.L., Rentz, D.M., Maye, J., Johnson, K.A., Growdon, J.H., 2012. Brain amyloid and cognition in Lewy body diseases. Mov. Disord. 27, 965–973.

Gomperts, S.N., Rentz, D.M., Moran, E., Becker, J.A., Locascio, J.J., Klunk, W.E., Mathis, C.A., Elmaleh, D.R., Shoup, T., Fischman, A.J., Hyman, B.T., Growdon, J.H., Johnson, K.A., 2008. Imaging amyloid deposition in Lewy body diseases. Neurology 71, 903–910.

Greve, D.N., Salat, D.H., Bowen, S.L., Izquierdo-Garcia, D., Schultz, A.P., Catana, C., Becker, J.A., Svarer, C., Knudsen, G.M., Sperling, R.A., Johnson, K.A., 2016. Different partial volume correction methods lead to different conclusions: an 18F-FDG-PET study of aging. Neuroimage 132, 334–343.

Greve, D.N., Svarer, C., Fisher, P.M., Feng, L., Hansen, A.E., Baare, W., Rosen, B., Fischl, B., Knudsen, G.M., 2014. Cortical surface-based analysis reduces bias and variance in kinetic modeling of brain PET data. Neuroimage 92, 225–236.

Habib, M., Mak, E., Gabel, S., Su, L., Williams, G., Waldman, A., Wells, K., Ritchie, K., Ritchie, C., O'Brien, J.T., 2017. Functional neuroimaging findings in healthy middle-aged adults at risk of alzheimer's disease. Ageing Res. Rev. 36, 88–104.

Hardy, J., 2002. The amyloid hypothesis of alzheimer's disease: progress and problems on the road to therapeutics. Science 297, 353–356.

Iglesias, J.E., Augustinack, J.C., Nguyen, K., Player, C.M., Player, A., Wright, M., Roy, N., Frosch, M.P., McKee, A.C., Wald, L.L., Fischl, B., Van Leemput, K., 2015. A computational atlas of the hippocampal formation using ex vivo, ultra-high resolution MRI: application to adaptive segmentation of in vivo MRI. Neuroimage 115, 117–137.

Jack, C.R., Knopman, D.S., Jagust, W.J., Petersen, R.C., Weiner, M.W., Aisen, P.S., Shaw, L.M., Vemuri, P., Wiste, H.J., Weigand, S.D., Lesnick, T.G., Pankratz, V.S., Donohue, M.C., Trojanowski, J.Q., 2013. Tracking pathophysiological processes in Alzheimer's disease: an updated hypothetical model of dynamic biomarkers. Lancet Neurol. 12, 207–216.

Josephs, K.A., Whitwell, J.L., Ahmed, Z., Shiung, M.M., Weigand, S.D., Knopman, D.S., Boeve, B.F., Parisi, J.E., Petersen, R.C., Dickson, D.W., Jack, C.R., 2008. Beta-amyloid burden is not associated with rates of brain atrophy. Ann. Neurol. 63, 204–212.

LaPoint, M.R., Chhatwal, J.P., Sepulcre, J., Johnson, K.A., Sperling, R.A., Schultz, A.P., 2017. The association between tau PET and retrospective cortical thinning in clinically normal elderly. Neuroimage 157, 612–622.

Mak, E., Gabel, S., Mirette, H., Su, L., Williams, G.B., Waldman, A., Wells, K., Ritchie, K., Ritchie, C., O'Brien, J., 2017a. Structural neuroimaging in preclinical dementia: from microstructural deficits and grey matter atrophy to macroscale connectomic changes. Ageing Res. Rev. 35, 250–264.

Mak, E., Gabel, S., Su, L., Williams, G.B., Arnold, R., Passamonti, L., Rodríguez, P.V., Surendranathan, A., Bevan-jones, W.R., Rowe, J.B., O'Brien, J.T., 2017b. Multimodal MRI investigation of volumetric and microstructural changes in the hippocampus and its subfields in mild cognitive impairment, Alzheimer's disease, and dementia with Lewy bodies. Int. Psychogeriatr. 29, 545–555.

Mak, E., Su, L., Williams, G.B., Watson, R., Firbank, M., Blamire, A., O'Brien, J., 2016. Differential atrophy of hippocampal subfields: a comparative study of dementia with lewy bodies and alzheimer disease. Am. J. Geriatr. Psychiatry 24, 136–143.

Mak, E., Su, L., Williams, G.B., Watson, R., Firbank, M., Blamire, A.M., O'Brien, J.T., 2015. Longitudinal assessment of global and regional atrophy rates in Alzheimer's disease and dementia with Lewy bodies. Neuroimage Clin. 7, 456–462.

Maruyama, M., Shimada, H., Suhara, T., Shinotoh, H., Ji, B., Maeda, J., Zhang, M.R., Trojanowski, J., Lee, V.Y., Ono, M., Masamoto, K., Takano, H., Sahara, N., Iwata, N., Okamura, N., Furumoto, S., Kudo, Y., Chang, Q., Saido, T., Takashima, A., Lewis, J., Jang, M.K., Aoki, I., Ito, H., Higuchi, M., 2013. Imaging of tau pathology in a tauopathy mouse model and in alzheimer patients compared to normal controls. Neuron 79, 1094–1108.

Matheson, G.J., Stenkrona, P., Cselényi, Z., Plavén-sigray, P., Halldin, C., Farde, L., Cervenka, S., 2017. Reliability of volumetric and surface-based normalisation and smoothing techniques for PET analysis of the cortex: a test-retest analysis using [11C]SCH-23390. Neuroimage 155, 344–353.

McKeith, I.G., Boeve, B.F., Dickson, D.W., Halliday, G., Aarsland, D., Attems, J., Ballard, C.G., Bayston, A., Beach, T.G., Chen-plotkin, A., Singleton, A., Taylor, A., 2017. Diagnosis and management of dementia with Lewy bodies: fourth consensus report of the DLB Consortium. Neurology 89, 1–13.

McKeith, I.G., Dickson, D.W., Lowe, J., Emre, M., O'Brien, J.T., Feldman, H., Cummings, J., Duda, J.E., Lippa, C., Perry, E.K., Aarsland, D., Arai, H., Ballard, C.G., Boeve, B., Burn, D.J., Costa, D., Del Ser, T., Dubois, B., Galasko, D., Gauthier, S., Goetz, C.G., Gomez-Tortosa, E., Halliday, G., Hansen, L.A., Hardy, J., Iwatsubo, T., Kalaria, R.N., Kaufer, D., Kenny, R.A., Korczyn, A., Kosaka, K., Lee, V.M.Y., Lees, A., Litvan, I.,

Londos, E., Lopez, O.L., Minoshima, S., Mizuno, Y., Molina, J.A., Mukaetova-Ladinska, E.B., Pasquier, F., Perry, R.H., Schulz, J.B., Trojanowski, J.Q., Yamada, M., Consortium on DLB, 2005. Diagnosis and management of dementia with Lewy bodies: third report of the DLB consortium. Neurology 65, 1863–1872.

Nedelska, Z., Ferman, T.J., Boeve, B.F., Przybelski, S.A., Lesnick, T.G., Murray, M.E., Gunter, J.L., Senjem, M.L., Vemuri, P., Smith, G.E., Geda, Y.E., Graff-Radford, J., Knopman, D.S., Petersen, R.C., Parisi, J.E., Dickson, D.W., Jack, C.R., Kantarci, K., 2015. Pattern of brain atrophy rates in autopsy-confirmed dementia with Lewy bodies. Neurobiol. Aging 36, 452–461.

Sarro, L., Senjem, M.L., Lundt, E.S., Przybelski, S.A., Lesnick, T.G., Graff-Radford, J., Boeve, B.F., Lowe, V.J., Ferman, T.J., Knopman, D.S., Comi, G., Filippi, M., Petersen, R.C., Jack, C.R., Kantarci, K., 2016. Amyloid-β deposition and regional grey matter atrophy rates in dementia with Lewy bodies. Brain 139, 2740–2750.

Schott, J.M., Bartlett, J.W., Barnes, J., Leung, K.K., Ourselin, S., Fox, N.C., 2010. Reduced sample sizes for atrophy outcomes in Alzheimer's disease trials: baseline adjustment. Neurobiol. Aging 31, 1452–1462.e2.

Shimada, H., Kitamura, S., Shinotoh, H., Endo, H., Niwa, F., Hirano, S., Kimura, Y., Zhang, M.-R., Kuwabara, S., Suhara, T., Higuchi, M., 2016. Association between Aβ and tau accumulations and their influence on clinical features in aging and Alzheimer disease spectrum brains: a [11C]PBB3-PET study. Alzheimers Dement. Diagn. Assess. Dis. Monit. 6, 11–20.

Shimada, H., Shinotoh, H., Hirano, S., Miyoshi, M., Sato, K., Tanaka, N., Ota, T., Fukushi, K., Irie, T., Ito, H., Higuchi, M., Kuwabara, S., Suhara, T., 2013. Beta-amyloid in lewy body disease is related to Alzheimer's disease-like atrophy. Mov. Disord. 28, 169–175.

Slattery, C.F., Zhang, J., Paterson, R.W., Foulkes, A.J.M., Mancini, L., Thomas, D.L., Modat, M., Toussaint, N., Cash, D.M., Thornton, J.S., Alexander, D.C., Ourselin, S., Fox, N.C., Zhang, H., Schott, J.M., 2015. Neurite orientation dispersion and density imaging (NODDI) in young-onset Alzheimer's disease and its syndromic variants. Alzheimers Dement. 11, P91.

Sluimer, J.D., van der Flier, W.M., Karas, G.B., Fox, N.C., Scheltens, P., Barkhof, F., Vrenken, H., 2008. Whole-brain atrophy rate and cognitive decline: longitudinal MR study of memory clinic patients. Radiology 248, 590–598.

Sperling, R.A., Rentz, D.M., Johnson, K.A., Karlawish, J., Donohue, M., Salmon, D.P., Aisen, P., 2014. The A4 study: stopping AD before symptoms begin? Sci. Transl. Med. 6, 228fs13.

Su, Y., D'Angelo, G.M., Vlassenko, A.G., Zhou, G., Snyder, A.Z., Marcus, D.S., Blazey, T.M., Christensen, J.J., Vora, S., Morris, J.C., Mintun, M.A., Benzinger, T.L.S., 2013. Quantitative analysis of PiB-PET with FreeSurfer ROIs. PLoS One 8, e73377.

Van Leemput, K., Bakkour, A., Benner, T., Wiggins, G., Wald, L.L., Augustinack, J., Dickerson, B.C., Golland, P., Fischl, B., 2009. Automated segmentation of hippocampal subfields from ultra-high resolution in vivo MRI. Hippocampus 19, 549–557.

West, M., Coleman, P., Flood, D., Troncoso, J., 1994. Differences in the pattern of hippocampal neuronal loss in normal ageing and Alzheimer's disease. Lancet 344, 769–772.

Wisse, L.E.M., Biessels, G.J., Heringa, S.M., Kuijf, H.J., Koek, D.L., Luijten, P.R., Geerlings, M.I., 2014. Hippocampal subfield volumes at 7T in early Alzheimer's disease and normal aging. Neurobiol. Aging 35, 2039–2045.

Yushkevich, P.A., Pluta, J.B., Wang, H., Xie, L., Ding, S.-L., Gertje, E.C., Mancuso, L., Kliot, D., Das, S.R., Wolk, D.A., 2015. Automated volumetry and regional thickness analysis of hippocampal subfields and medial temporal cortical structures in mild cognitive impairment. Hum. Brain Mapp. 36, 258–287.